Successive superconducting transitions and Anderson localization effect in Ta_2S_2C

Jürgen Walter*
Department of Materials Science and Processing, Graduate School of Engineering, Osaka University, 2-1, Yamada-oka, Suita, 565-0879, Japan

Itsuko S. Suzuki† and Masatsugu Suzuki‡
Department of Physics, State University of New York at Binghamton, Binghamton, New York 13902-6016, USA
(Received 24 September 2003; revised manuscript received 29 March 2004; published 31 August 2004)

A complex carbide Ta_2S_2C consists of van der Waals (vdw)-bonded layers with a stacking sequence along the *c* axis: ···C-Ta-S-vdw-S-Ta-C-···. The magnetic properties of this compound have been studied from dc and ac magnetic susceptibility. Ta_2S_2C undergoes successive superconducting transitions of a hierachical nature at $T_{cl}=3.61\pm0.01$ K [$H_{c1}^{(l)}(0)=28\pm2$ Oe and $H_{c2}^{(l)}(0)=7.7\pm0.2$ kOe] and $T_{cu}=8.9\pm0.1$ K [$H_{c2}^{(u)}(0)=14.0\pm0.5$ kOe]. The intermediate phase between T_{cu} and T_{cl} is an intragrain superconductive state occurring in the Ta-C layers in Ta_2S_2C. The low temperature phase below T_{cl} is an intergrain superconductive state. The magnetic susceptibility at *H* well above 10 kOe is described by a sum of a diamagnetic susceptibility and a Curie-type behavior. The latter is due to the localized magnetic moments of conduction electrons associated with the Anderson localization effect, occurring in the 1T-TaS_2 type structure in Ta_2S_2C.

DOI: 10.1103/PhysRevB.70.064519 PACS number(s): 74.25.Ha, 74.81.Bd, 74.25.Dw, 73.20.Fz

I. INTRODUCTION

Ta_2S_2C has a unique layered structure, where a sandwiched sequence of C-Ta-S-vdw-S-Ta-C is periodically stacked along the *c* axis.[1–10] A van der Waals (vdw) gap is between adjacent S layers. There are two polytypes: 1T-Ta_2S_2C (space group $P\bar{3}m1$, $a=3.265$ Å, $c=8.537$ Å) and 3R-Ta_2S_2C (space group $R\bar{3}m$, $a=3.276$ Å, $c=25.62$ Å). In the Ta-C-Ta layer (for simplicity Ta-C layers are used hereafter), each [Ta_6C] octahedron shares six of its 12 edges with adjacent octahedra and the corner Ta atom is shared by three octahedra. This edge linking of [Ta_6C] octahedra is the common structural feature of transition metal carbides. Relatively weak vdw interactions between S layers give this compound a graphitic character. The structure of Ta_2S_2C can be viewed as a structural sum of Ta-C layers and TaS_2. The structural part corresponding to Ta-C layers is represented by [Ta_6C] octahedra and the structural part corresponding to TaS_2 is identical to the atom disposition of either 1T-TaS_2 in the case of 3R-Ta_2S_2C or a hypothetical 2H_b-TaS_2 (MoS_2-type) in the case of 1T-Ta_2S_2C. X-ray photoelectron core level spectra[10] of Ta_2S_2C show that the binding energy of carbon is close to that in a graphene sheet on (111) face of Ta rather than carbon in tantalum carbides (TaC, Ta_2C). The binding energy of sulfur is close to that in 1T-TaS_2. The structure of the Ta-C layers in Ta_2S_2C is different from that of the bulk TaC (cubic) and Ta_2C (hexagonal) which are cubic compounds and do not show any layered structure.

In this paper we have undertaken an extensive study on the magnetic properties of Ta_2S_2C from SQUID (superconducting quantum interference device) dc and ac magnetic susceptibility. We show that this compound undergoes successive superconducting phase transitions at T_{cl} (=3.61±0.01 K) and T_{cu} (=8.9±0.1 K). The intermediate phase between T_{cl} and T_{cu} is an intragrain superconductive state, while the low temperature phase below T_{cl} is an intergrain superconductive state. The superconducting properties of Ta_2S_2C are compared with those of Nb_2S_2C type-II superconductor with a critical temperature $T_c=7.6$ K.[11] In the presence of a magnetic field (*H*) well above 10 kOe, the magnetic susceptibility is described by a sum of a Curie-type behavior and a diamagnetic susceptibility. We show that the Curie-type behavior is due to localized magnetic moments of conduction electrons associated with the Anderson localization effect, which may occur in the 1T-TaS_2 type structure in Ta_2S_2C.

The pristine TaC_{1-x} is a superconductor with a fairly high T_c (=9.7 K) for $x\approx1$, but for $x\approx0.8$ no superconductivity is found.[12,13] The small change of the Fermi surface due to the nonstoichiometry of the carbides considerably reduces the bulk phonon anomaly (dip) resulting in the reduction of T_c.[14] Recently we have shown that Ta-graphite having a *c*-axis stacking sequence -C-Ta-C-Ta-C-··· undergoes a superconducting transition around 10 K.[15]

In the pristine 1T-TaS_2 the charge density wave (CDW) becomes commensurate with an undistorted host lattice in a first order transition below 200 K.[16] The electrical resistivity increases about ten fold at the 200 K transition and below 2 K the resistivity diverges following the relation $\rho=\rho_0\exp[(T_0/T)^n]$ with $n=1/3$, where ρ_0 is a constant resistivity and T_0 is a characteristic temperature.[17] This is characteristic of the Anderson localization of the conduction electrons due to a random potential. The susceptibility shows a Curie-type behavior due to the localized magnetic moments of conduction electrons.[18,19]

II. EXPERIMENTAL PROCEDURE

Powdered samples of Ta_2S_2C were prepared by Pablo Wally. The detail of the synthesis and structure is described by Wally and Ueki.[6] X-ray powder diffraction pattern shows

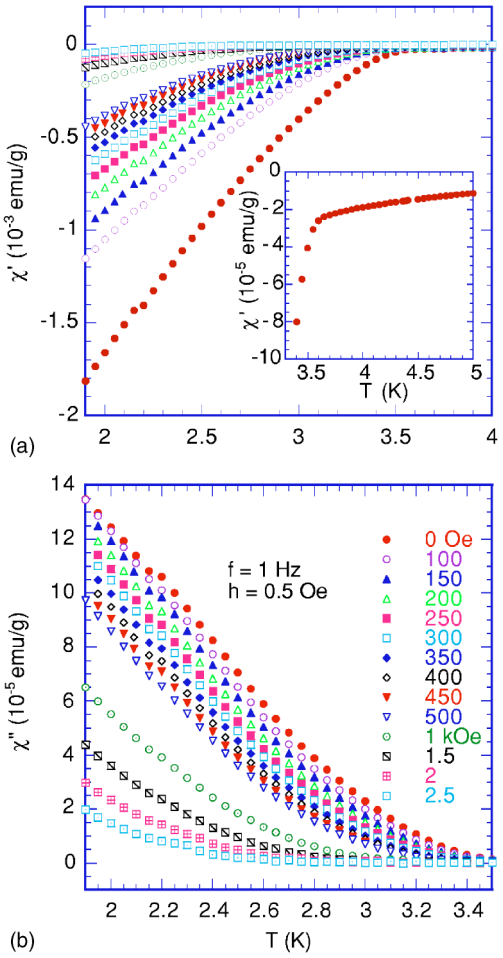

FIG. 1. (Color online) T dependence of (a) χ' and (b) χ'' with and without H for Ta_2S_2C. $h=0.5$ Oe. $f=1$ Hz. The inset shows the detail of χ' at $H=0$ around T_{cl}.

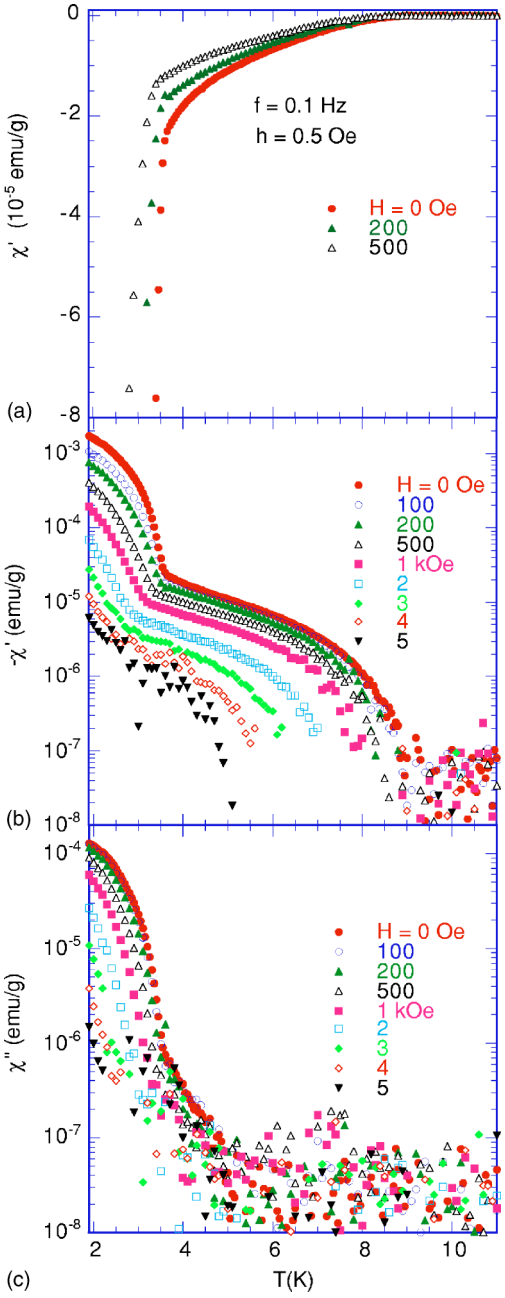

FIG. 2. (Color online) T dependence of (a) χ' (b) $-\chi'$ and (c) χ'' with and without H. $f=0.1$ Hz. $h=0.5$ Oe.

that Ta_2S_2C sample consists of a 3R phase as a majority phase and a 1T phase as a minority phase.[6] The sample characterization was carried out by scanning tunneling microscopy[9] and x-ray photoelectron spectroscopy.[10] The measurements of dc and ac magnetic susceptibility were carried out using a SQUID magnetometer (Quantum Design MPMS XL-5). A polycrystalline powdered sample (mass 253.2 mg) was used in the present work. Before setting up a sample at 298 K, a remnant magnetic field was reduced to less than 3 mOe using an ultralow field capability option. For convenience, hereafter this remnant field is noted as the state $H=0$. The detail of the measurements of dc and ac magnetic susceptibility is described in Sec. III.

III. RESULT

A. χ' and χ''

Figure 1 shows the T dependence of the ac magnetic susceptibility [(a) the dispersion χ' and (b) the absorption χ''], where the ac frequency f (=1 Hz) and the magnitude of the ac field ($h=0.5$ Oe) are used. The T dependence of χ' and χ'' is strongly dependent on H. The sign of χ' is negative at least for $1.9<T<5$ K, while the sign of χ'' is positive. For $H=0$ [see the inset of Fig. 1(a)], χ' increases with increasing T. It shows a kink at a critical temperature T_{cl} (=3.61 K) where the derivative $d\chi'/dT$ undergoes a discontinuous jump. The system undergoes a superconducting transition at T_{cl}. The absorption χ'' at $H=0$ shows a drastic decrease around T_{cl} [see Fig. 2(c) for detail]. It shows a tail above T_{cl} and is reduced to zero around 5 K. The temperature at which the tangential line χ'' vs T with the steepest slope intersects the $\chi''=0$ axis coincides with T_{cl}.

In Figs. 2(a)–2(c) we show the T dependence of χ' and χ'' at $f=0.1$ Hz and $h=0.5$ Oe for $0\leqslant H\leqslant 5$ kOe. The dispersion χ' shows a kink-like behavior at $T_{cl}(H)$, increases with

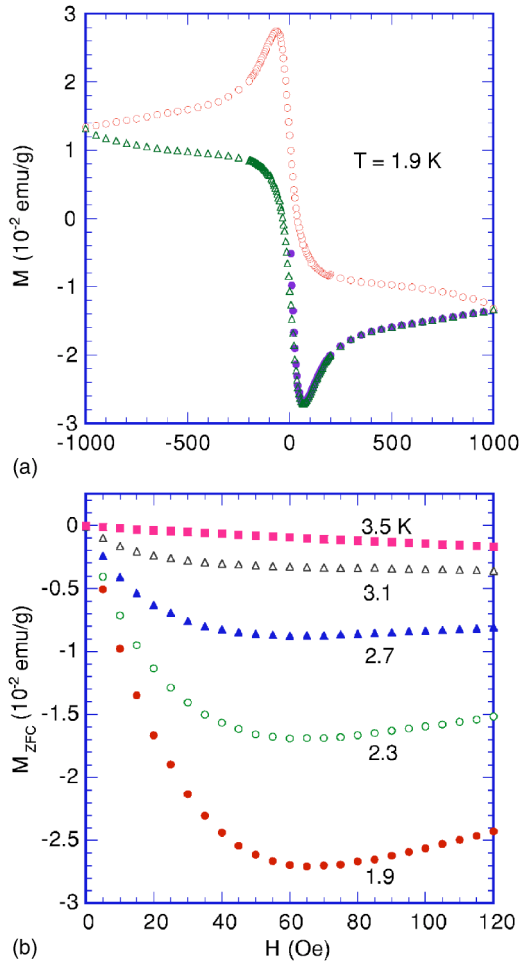

FIG. 3. (Color online) (a) M-H loop at 1.9 K. (b) H dependence of M_{ZFC} at various T.

further increasing T and reduces to zero at $T_{cu}(H)$. In the plot of $(-\chi')$ vs T in Fig. 2(b), two steplike changes are clearly observed at $T_{cl}(H)$ and $T_{cu}(H)$. Although χ'' drastically decreases at $T_{cl}(H)$ with increasing T [see Fig. 2(c)], no drastic change in χ'' is observed at $T_{cu}(H)$ in contrast to the case of $-\chi'$ vs T. The critical temperatures $T_{cl}(H)$ and $T_{cu}(H)$ decrease with increasing H, forming the H-T phase diagram (see Sec. III E).

B. M-H loop

Figure 3(a) shows the hysteresis loop of the magnetization M at $T=1.9$ K. After the sample was quenched from 298 to 1.9 K at $H=0$, the measurement was carried out with varying H from 0 to 1 kOe at T, from $H=1$ to -1 kOe, and from $H=-1$ to 1 kOe. The M-H curve at 1.9 K shows a large hysteresis and a remnant magnetization. Structural imperfections or defect in the sample may play a role of flux pinning, resulting in a inhomogeneous type-II superconductor. Figure 3(b) shows typical data of zero-field cooled (ZFC) magnetization M_{ZFC} vs H at various T. Before each measurement, the sample was kept at 20 K and $H=0$ for 20 min and then it was quenched from 20 K to T (<4 K). The magnetization M_{ZFC} at T was measured with increasing H ($0 \leqslant H \leqslant 120$ Oe). The magnetization M_{ZFC} exhibits a single local minimum at a characteristic field for $T<T_{cl}$, shifting to the low-H side with increasing T. The lower critical field $H_{c1}^{(l)}(T)$ is defined not as the first minimum point of the M_{ZFC} vs H, but as the first deviation point from the linear portion due to the penetration of magnetic flux into the sample: typically, $H_{c1}^{(l)}(T=1.9\ \mathrm{K})=20$ Oe and $H_{c1}^{(l)}(T=2.7\ \mathrm{K})=12$ Oe. The least-squares fit of the data of $H_{c1}^{(l)}$ vs T to a conventional relation[20] $H_{c1}^{(l)}(T)=H_{c1}^{(l)}(0)[1-(T/T_{cl})^2]$ yields $H_{c1}^{(l)}(0)=28\pm2$ Oe.

C. χ_{ZFC} and χ_{FC}

The measurements of χ_{ZFC} $(=M_{\mathrm{ZFC}}/H)$ and χ_{FC} $(=M_{\mathrm{FC}}/H)$ were carried out as follows, where M_{FC} is the field-cooled (FC) magnetization. After annealing at 50 K for 1200 s in the absence of H, the sample was quenched from 50 to 1.9 K. The magnetic field H was applied at 1.9 K and then χ_{ZFC} was measured with increasing T. The sample was again heated up and annealed at 50 K for 1200 s in the presence of H. Then χ_{FC} was measured with decreasing T. Figures 4(a) and 4(b) show the T dependence of χ_{ZFC}, χ_{FC}, and $\delta\chi$ at $H=1$ Oe, where $\delta\chi=\chi_{\mathrm{FC}}-\chi_{\mathrm{ZFC}}$. The scale of the susceptibility is enlarged in Fig. 4(b). The susceptibility χ_{ZFC} (χ_{FC}) exhibits a kink at T_{cl} (=3.61 K), where $d\chi_{\mathrm{ZFC}}/dT$ $(d\chi_{FC}/dT)$ undergoes a drastic decrease. The deviation of χ_{ZFC} from χ_{FC} is clearly seen below T_{cl} (=3.61 K), indicating that the extra magnetic flux is trapped during the FC process. Between T_{cl} and T_{cu} (=8.9 K), $\delta\chi$ is still positive but almost equal to zero. The sign of χ_{ZFC} (χ_{FC}) changes from negative to positive at T_{cu}. Similar behavior is also observed at $H=20$ Oe as shown in Figs. 4(c) and 4(d). Figure 5 shows the T dependence of $\delta\chi$ at various H. The value of $\delta\chi$ at fixed T decreases with increasing H. The difference $\delta\chi$ undergoes a drastic decrease at $T_{cl}(H)$.

The minimum value of χ_{ZFC} at $H=1$ Oe is -1.7×10^{-3} emu/g at 1.9 K, while the minimum value of χ' at $H=0$ is -1.8×10^{-3} emu/g at 1.9 K. Using the value of χ' at 1.9 K ($\approx-1.8\times10^{-3}$ emu/g) and the calculated density for 3R-Ta_2S_2C ($\rho_{\mathrm{cal}}=9.23\ \mathrm{g/cm^3}$),[1] the fraction of flux expulsion relative to complete diamagnetism ($\chi_0=-1/4\pi=-0.0796\ \mathrm{emu/cm^3}$) is estimated as 21%, suggesting that the system consists of small grains. This is in contrast to 38% of the diamagnetic volume fraction reported for Nb_2S_2C by Sakamaki *et al.*[11]

Figures 6(a) and 6(b) show the T dependence of χ_{ZFC} at various H, where the measurement was carried out between 1.9 and 11 K with increasing T. There is a drastic increase in the diamagnetic contribution in χ_{ZFC} associated with the superconducting transition at $T_{cl}(H)$. Nevertheless, a diamagnetic contribution in χ_{ZFC} still remains above $T_{cl}(H)$. The susceptibility χ_{ZFC} increases with further increasing T, and reduces to a zero at an upper critical temperature $T_{cu}(H)$. For $H=500$ Oe, for example, χ_{ZFC} exhibits a kink at $T_{cl}(H)$. The sign of χ_{ZFC} changes from negative to positive around 9 K with increasing T. At $H=5$ kOe, χ_{ZFC} is positive at least between 1.9 and 6 K, showing a broad peak at 2.65 K. At $H=10$ kOe, χ_{ZFC} decreases with increasing T, showing a

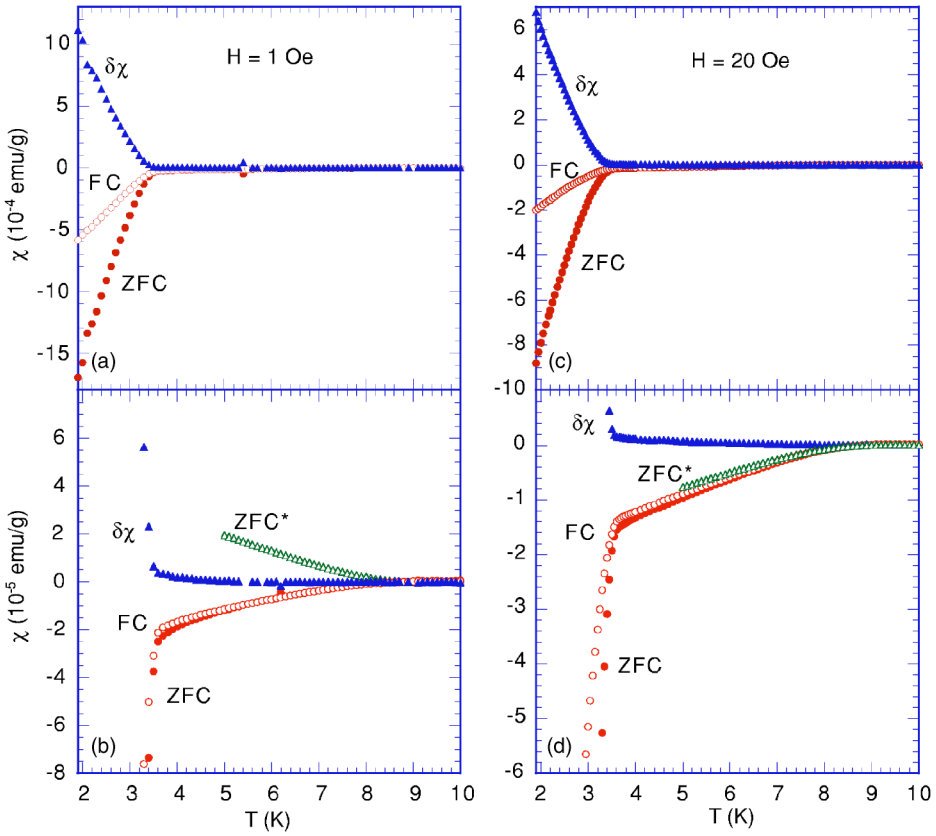

FIG. 4. (Color onine) T dependence of χ_{ZFC}, χ_{FC}, and $\delta\chi$ ($=\chi_{\mathrm{FC}}-\chi_{\mathrm{ZFC}}$). (a) and (b) for $H=1$ Oe. (c) and (d) for $H=20$ Oe. T dependence of χ^{*}_{ZFC} ($5\leqslant T\leqslant 10$ K) is also shown for comparison. The definition of χ^{*}_{ZFC} is given in Sec. III D.

Curie-type behavior. Figure 7(a) shows the T dependence of $\delta\chi$ at various H. The magnitude of $\delta\chi$ between $T_{cl}(H)$ and $T_{cu}(H)$ is very small compared to that below $T_{cl}(H)$, but still shows the irreversible effect of magnetization. The difference $\delta\chi$ at fixed H decreases with increasing T and reduces to zero at $T_{cu}(H)$. Note that $\delta\chi$ at fixed T (for example 5 K) increases with increasing H, showing a maximum around $H=500$ Oe, and decreases with further increasing H. This feature is in contrast to the H dependence of $\delta\chi$ below $T_{cl}(H)$, which decreases with increasing H. Figure 7(b) shows the T dependence of the derivative $\mathrm{d}\chi_{\mathrm{ZFC}}/\mathrm{d}T$ for

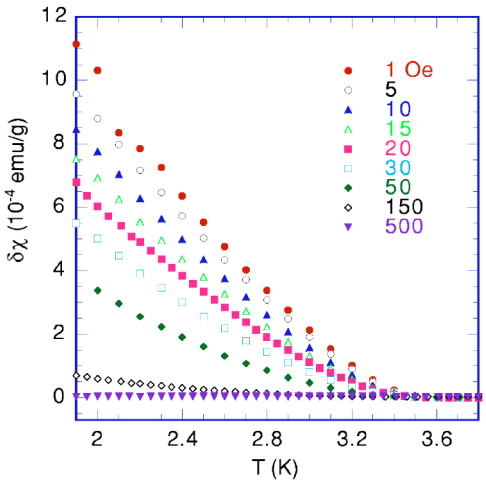

FIG. 5. (Color online) T dependence of $\delta\chi$ ($=\chi_{\mathrm{FC}}-\chi_{\mathrm{ZFC}}$) at various H around T_{cl}.

5 Oe$\leqslant H\leqslant$10 kOe. Clearly $\mathrm{d}\chi_{\mathrm{ZFC}}/\mathrm{d}T$ at low H undergoes two steplike changes around $T_{cl}(H)$ and $T_{cu}(H)$. The critical temperatures $T_{cl}(H)$ and $T_{cu}(H)$ decrease with increasing H, forming the H-T phase diagram (see Sec. III E).

D. χ^{*}_{ZFC} in a quasiequilibrium state

Here we present our peculiar results on the T dependence of χ^{*}_{ZFC}. The method of the measurement for χ^{*}_{ZFC} is slightly different from that for the conventional χ_{ZFC}. First, the sample was annealed at 50 K for 1200 s in the absence of H and then it was quenched to 1.9 K. After the sample was kept at 1.9 K for 100 s in the presence of fixed H, it was quickly heated up to T_0 between T_{cl} and T_{cu}. Then χ^{*}_{ZFC} was measured with increasing T from T_0 to 11 K. Figures 8(a)–8(d) show the T dependence of χ^{*}_{ZFC}, χ_{ZFC}, and χ_{FC} at various H (5, 10, 30, and 50 Oe), where $T_0=5$ K. The T dependence of χ^{*}_{ZFC} at the same H is independent of T_0 when T_0 is between 4 and 8 K. The data of χ^{*}_{ZFC} vs T at $H=1$ and 20 Oe are shown in Figs. 4(b) and 4(d), respectively. The susceptibility χ^{*}_{ZFC} increases with increasing T and reduces to zero at $T_{cu}(H)$. The magnitudes of χ_{ZFC}, χ^{*}_{ZFC}, and χ_{FC} at the same T are strongly dependent on H: $\chi^{*}_{\mathrm{ZFC}}>\chi_{\mathrm{FC}}>\chi_{\mathrm{ZFC}}$ for $H=1$–30 Oe, $\chi_{\mathrm{FC}}>\chi^{*}_{\mathrm{ZFC}}>\chi_{\mathrm{ZFC}}$ for $H=50$ Oe, and $\chi_{\mathrm{FC}}>\chi^{*}_{\mathrm{ZFC}}=\chi_{\mathrm{ZFC}}$ for $H=100$ and 150 Oe (the data are not shown in Fig. 8). Note that χ^{*}_{ZFC} at $H=1$ Oe [see Fig. 4(b)], whose sign is positive, decreases with increasing T and reduces to zero at T_{cu}. Between T_{cl} and T_{cu}, the space of states is divided into at least three states, the ZFC, ZFC*, and FC state. The system lies in the FC states under the cooling from 11 K, the ZFC state under the slow heating from 1.9 K, and

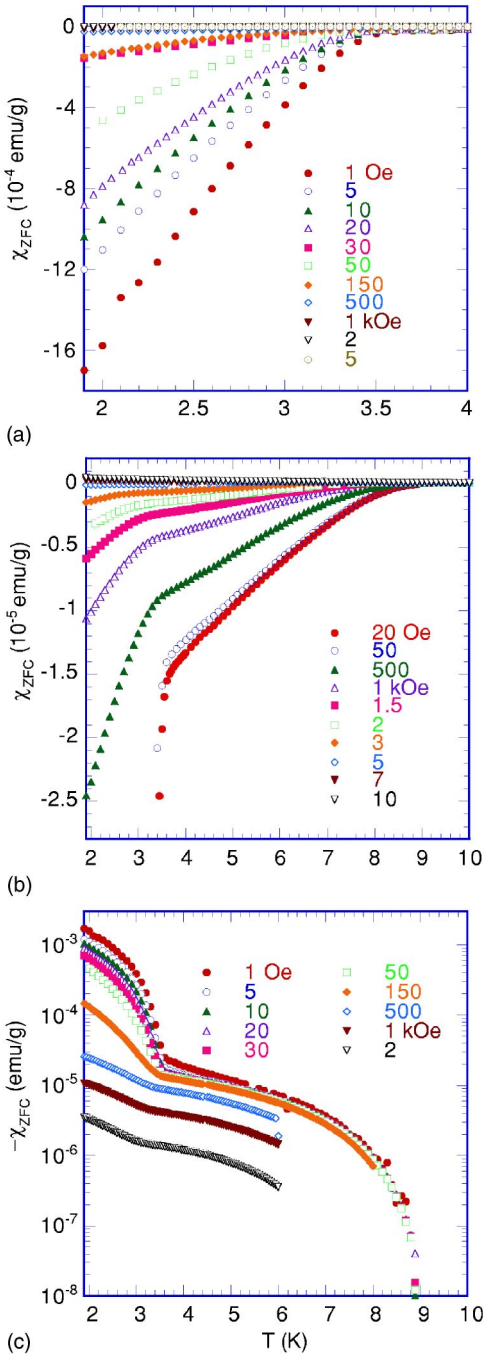

FIG. 6. (Color online) T dependence of (a) and (b) χ_{ZFC} and (c) $-\chi_{\mathrm{ZFC}}$ at various H.

the ZFC* state under the rapid heating from 1.9 K. The value of H (=30 Oe) is slightly higher than the lower critical field $H_{c1}^{(l)}(T=1.9\ \mathrm{K})=20$ Oe. The susceptibility of each state provides a measure for the corresponding induced magnetic flux density B which is trapped in the superconducting grains: $B=H+4\pi M$. The inequality $\chi_{\mathrm{ZFC}}^{*}>\chi_{\mathrm{FC}}$ indicates that the induced magnetic flux density (or the number of fluxoids over the system) in the ZFC* state is higher than that in the FC state for $H<30$ Oe. Such a relatively high flux density in the ZFC* state may be due to a flux compression as a result of the rapid redistribution of the grain-pinned vortices which

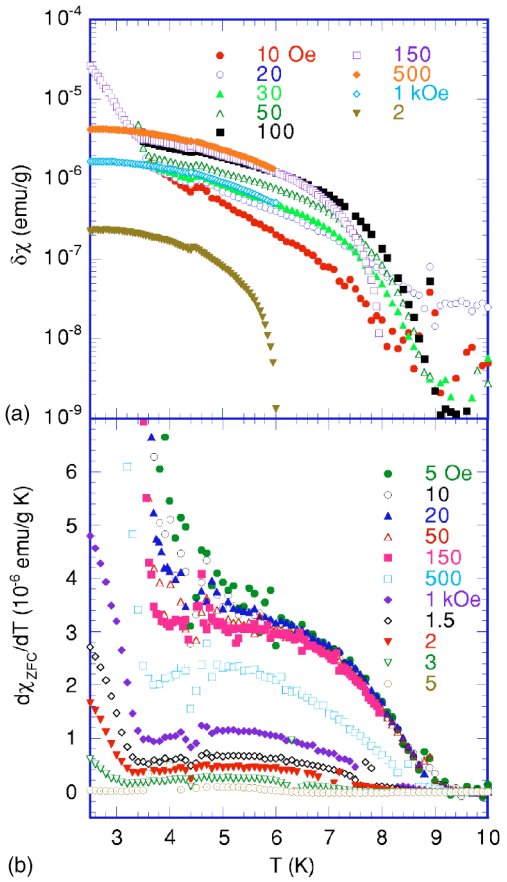

FIG. 7. (Color online) T dependence of (a) $\delta\chi$ and (b) $\mathrm{d}\chi_{\mathrm{ZFC}}/\mathrm{d}T$ at various H for $T_{cl}\leqslant T\leqslant T_{cu}$.

occurs during a change of T from 1.9 K to T_0. This effect exists only at low H. In this sense, the present effect is similar to the paramagnetic Meissner effect observed in χ_{FC} of the pristine Nb:[21,22] χ_{FC} at low H becomes positive below the superconducting transition temperature. According to Koshelev and Larkin,[23] the surface supercurrent inhomogeneously traps the magnetic flux in the sample interior, as a vortex. In Sec. IV A we discuss a possible distribution of vortices around the grains in the ZFC and FC states below T_{cl} and between T_{cl} and T_{cu}.

E. *H-T* diagram

Figure 9 shows the H-T phase diagram, where $T_{cl}(H)$ is determined from the data of χ' vs T and χ'' vs T, and $T_{cu}(H)$ is determined from the data of χ_{ZFC} vs T. These lines correspond to the lines $H_{c2}^{(l)}(T)$ and $H_{c2}^{(h)}(T)$. The least squares-fit of the data of H vs T for the line $H_{c2}^{(l)}(T)$ to a conventional relation $H_{c2}^{(l)}(T)=H_{c2}^{(l)}(0)[1-(T/T_{cl})^2]$ yields $H_{c2}^{(l)}(0)=7.7\pm0.2$ kOe and $T_{cl}=3.61\pm0.01$ K, where the data of χ' vs T and χ'' vs T are used. The value of $H_{c2}^{(l)}(0)$ thus obtained is comparable to that estimated using an empirical relation given by Werhammer *et al.*,[24] $H_{c2}^{(l)}(T=0\ \mathrm{K})=-0.69T_{cl}(\mathrm{d}H_{c2}^{(l)}/\mathrm{d}T)_{T=T_{cl}}$. In fact, the value of $H_{c2}^{(l)}(0)$ is calculated as 6.3 ± 0.2 kOe, where we use $T_{cl}=3.61$ K and a slope $(\mathrm{d}H_{c2}^{(l)}/\mathrm{d}T)_{T_{cl}}=-2500\pm189$ Oe/K

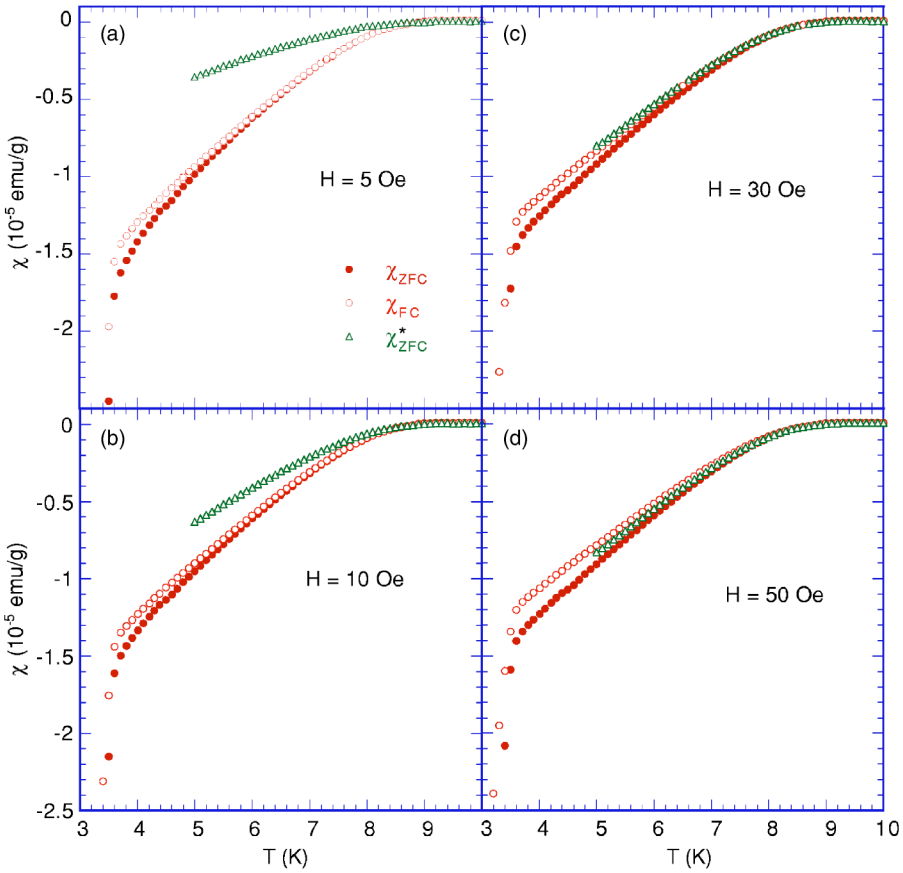

FIG. 8. (Color online) (a)–(d) T dependence of χ^*_{ZFC}, χ_{ZFC}, and χ_{FC} at various low H. The definition of χ^*_{ZFC} is given in Sec. III D. The measurement of χ^*_{ZFC} was made with increasint T from T_0 (=5 K) after the sample was quickly heated from 1.9 K (ZFC state) to T_0. χ_{ZFC} and χ_{FC} were measured between 1.9 and 10 K.

obtained from the linear relation in $H^{(l)}_{c2}$ vs T in the vicinity of $T=T_{cl}$ and $H^{(l)}_{c2}=0$.

The coherence length ξ and the magnetic penetration depth λ are related to $H^{(l)}_{c1}(0)$ and $H^{(l)}_{c2}(0)$ through relations

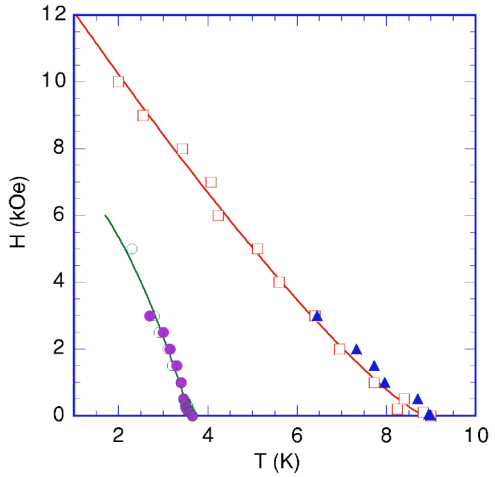

FIG. 9. (Color online) H-T phase diagram, where $T_{cl}(H)$ is determined from the measurements of χ' ($f=1$ Hz) vs T (•) and χ'' ($f=1$ Hz) vs T (◦), and $T_{cu}(H)$ is determined from the measurements of χ' ($f=0.1$ Hz) vs T (□) and χ_{ZFC} vs T (▲). Solid lines are least-squares fitting curves for the data of $T_{cl}(H)$ and $T_{cu}(H)$ to the form $H^{(l)}_{c2}(T)=H^{(l)}_{c2}(0)[1-(T/T_{cl})^2]$ and $H^{(u)}_{c2}(T)=H^{(u)}_{c2}(0)(1-T/T_{cu})^{\alpha}$. The fitting parameters are given in the text. $T_{cl}=3.61$ K. $T_{cu}=8.9$ K.

$H^{(l)}_{c1}(0)=\Phi_0/(2\pi\xi^2)$ and $H^{(l)}_{c1}(0)=(\Phi_0/4\pi\lambda^2)\ln(\lambda/\xi)$, where Φ_0 ($=2.0678\times10^{-7}$ Gauss cm^2) is the fluxoid.[20] When the values of $H^{(l)}_{c1}(0)$ (=27.7 Oe) and $H^{(l)}_{c2}(0)$ (=7730 Oe) are used, the values of the Ginzburg-Landau parameter κ ($=\lambda/\xi$), λ and ξ can be estimated as $\kappa=20.5\pm0.3$, $\xi=210\pm10$ Å, and $\lambda=4200\pm100$ Å. Our results of T_{cl}, $H^{(l)}_{c1}(0)$, $H^{(l)}_{c2}(0)$, κ, λ, and ξ in Ta_2S_2C thus obtained are compared to those in Nb_2S_2C:[11] $T_c=7.6$ K, $H_{c1}(0)=227\pm4$ Oe and $H_{c2}(0)=9950\pm180$ Oe, $\kappa=6.37$, $\xi=182\pm2$ Å, and $\lambda=1160\pm20$ Å. Both the pristine Nb and Ta are superconductive elements with the critical temperatures and $T_c(\mathrm{Nb})=9.25\pm0.02$ K and $T_c(\mathrm{Ta})=4.47\pm0.04$ K,[20] and have a body-centered cubic structure. We find that the ratio $T_c(Nb_2S_2C)/T_c(Ta_2S_2C)(=2.11)$ is close to the ratio $T_c(\mathrm{Nb})/T_c(\mathrm{Ta})$ (=2.06). The values of T_c and H_{c2} for Ta_2S_2C are comparable to those of $2H_a$-TaS_xSe_{2-x} ($0.4<x<1.8$): $T_c=3.9$ K and $H_{c2}=6.7$ kOe for $x=0.8$, $T_c=3.7$ K and $H_{c2}=9-11$ kOe for $x=1$, $T_c=3.9$ K and $H_{c2}=11.5-12.8$ kOe at $x=1.2$.[25]

What kind of the superconductivity occurs at $T_{cu}(H)$? Our data of $T_{cu}(H)$ vs H cannot be well described by a conventional form $[H^{(u)}_{c2}(T)=H^{(u)}_{c2}(0)[1-(T/T_{cu})^2]$. An upward curvature in $H^{(u)}_{c2}$ vs T indicates that $H^{(u)}_{c2}(T)$ can be described by $H^{(u)}_{c2}(0)(1-T/T_{cu})^{\alpha}$ with an exponent α being larger than 1. In fact the least squares fit of the data of $H^{(u)}_{c2}$ vs T to this form yields the parameters $H^{(u)}_{c2}(0)=14.0\pm0.5$ kOe, $T_{cu}=8.9\pm0.1$ K, and $\alpha=1.23\pm0.07$ for Ta_2S_2C. The origin of the superconductivity at $T_{cu}(H)$ may be due to Ta-C layers in Ta_2S_2C. According to Giorgi *et al.*,[12] the critical temperature

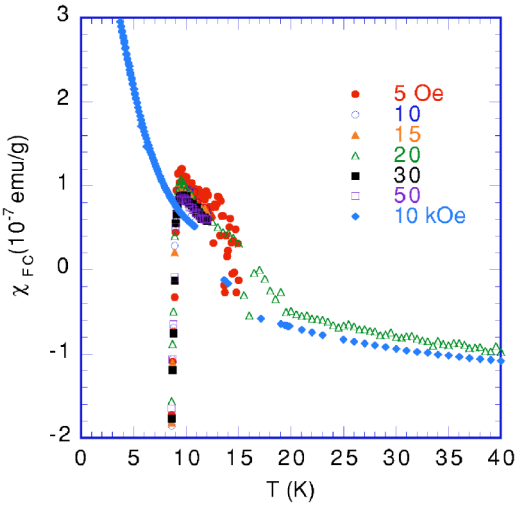

FIG. 10. (Color online) T dependence of χ_{FC} at various H near T_{cu}.

T_c of the pristine TaC_{1-x} increases with decreasing x and is equal to 9.0 K at $x=0.019$. Fink *et al.*[13] have reported that the values of H_{c1} and H_{c2} at $T=1.2$ K for TaC are 220 Oe and 4.6 kOe. These values are on the same order as the values of T_{cu} and $H_{c2}^{(u)}(0)$ in Ta_2S_2C. The origin of the superconductivity at T_{cl} and T_{cu} will be discussed in Sec. IV A.

F. χ_{ZFC} and χ_{FC} at high H and high T

In Fig. 10 we show the T dependence of χ_{FC} at various H. The susceptibility χ_{FC} (also χ_{ZFC}) at $H=20$ Oe shows a sharp peak around 9.5 K and decreases with further increasing T. The sign of χ_{FC} changes from positive to negative around 16 K. The discontinuous jump of χ observed in the vicinity of $\chi=0$ is an artifact due to the SQUID measurement. In contrast, χ_{FC} $(=\chi_{\mathrm{ZFC}})$ at $H=10$ kOe decreases with increasing T from 1.9 K and merges to the curves of χ_{FC} at $H=20$ Oe above 9.5 K.

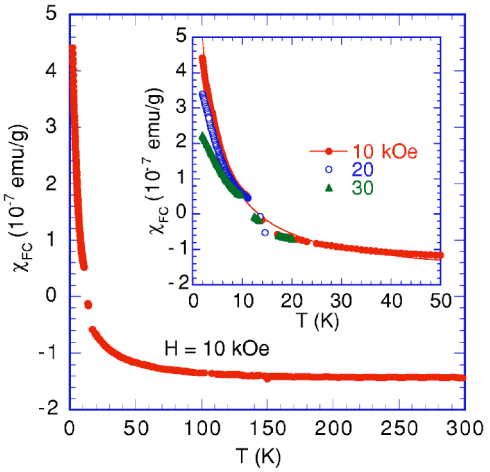

FIG. 11. (Color online) T dependence of χ_{FC} at $H=10$ kOe. The inset shows the T dependence of χ_{FC} at $H=10$, 20, and 30 kOe. The solid line in the inset denotes the least-squares fitting curve to Eq.(1). The fitting parameters are given in the text.

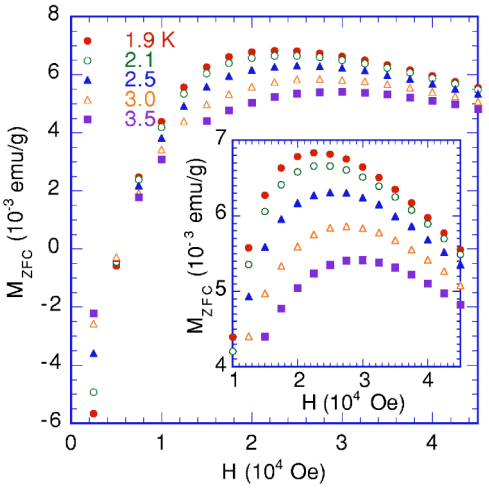

FIG. 12. (Color online) Magnetization M_{ZFC} as a function of H at low T.

Figure 11 shows the T dependence of χ_{FC} at $H=10$ kOe for $1.9 \leqslant T \leqslant 298$ K. The susceptibility χ consists of a diamagnetic susceptibility and a Curie-type susceptibility. The susceptibility χ_{FC} slightly decreases with increasing T above 20 K and becomes a negative constant (diamagnetic susceptibility) above 150 K: $\chi_d=(-1.44\pm0.01)\times10^{-7}$ emu/g at 298 K. Similar T dependence of χ is observed in 1T-TaS_2 below 150 K.[18,19] A steplike change χ near 200 K for 1T-TaS_2 is due to the CDW transition between a high-temperature incommensurate phase and a low-temperature commensurate phase. As seen in Fig. 11 there is no such anomaly above 20 K in Ta_2S_2C. The inset of Fig. 11 shows the T dependence of χ_{FC} at $H=10$, 20, and 30 kOe. The susceptibility is strongly dependent on H below 10 K, indicating that M_{FC} is nonlinear in H (see also the data of M_{ZFC} vs H in Fig. 12). Note that the discontinuous jump of χ_{FC} observed in the vicinity of $\chi_{\mathrm{FC}}=0$ is an artifact due to the SQUID measurement. Almost all the data between 10 and 16 K are removed from the figure. The least-squares fit of the data of χ_{FC} vs T at $H=10$ kOe for $4 \leqslant T \leqslant 43$ K to

$$\chi_{\mathrm{FC}} = \chi_0 + C/(T-\Theta), \tag{1}$$

yields the T-independent susceptibility $\chi_0=(-1.80\pm0.02)\times10^{-7}$ emu/g, the Curie-Weiss constant $C=(2.91\pm0.04)\times10^{-6}$ emu K/g, and the Curie-Weiss temperature $\Theta=-2.37\pm0.07$ K. The magnitude of χ_0 is slightly larger than that of χ_d determined above. The susceptibility χ_{FC} consists of a Curie-type behavior at low T and a diamagnetic contribution at high T. We assume that the Curie-type behavior is due to the localized electron spins having the effective magnetic moment $P_{\mathrm{eff}}=g[S(S+1)]^{1/2}\mu_B=\sqrt{3}\mu_B$, where the Landé g-factor $g=2$ and the spin $S=1/2$. This localized magnetic moment could be related to the Anderson localization (see Sec. IV B). Through the repulsive Coulomb interaction between the electrons, a singly occupied state exists in the vicinity of ϵ_F. Then the number of spins per gram of Ta_2S_2C (N_g) can be estimated as $N_g=4.67\times10^{18}$/g (or $4.3\times10^9/\mathrm{cm}^3$) from the Curie-Weiss constant. In summary, the superconductivity below T_{cl}, which is dominant at low H, is

weakened as H increases and overcome by the localization effect at high H well above $H_{c2}^{(l)}(0)$.

There may be another possibility that the Curie-Weiss behavior is due to magnetic impurities (for example, Fe^{2+}), which may be contained in original Ta (typically 15 ppm Fe in the pristine 1T-TaS_2).[19] However, this possibility may be ruled out in the following way. If each Fe^{2+} ion has the effective magnetic moment ($=5.4\mu_B$), then the number of Fe^{2+} spins per gram of Ta_2S_2C is estimated as $N_g=2.0\times10^{19}$/g. The magnitude of Fe^{2+} impurities is estimated as 1800 ppm, which is too large compared to ≈15 ppm as major metallic impurities in Ta_2S_2C. Similar Curie-Weiss behavior is observed in the susceptibility of 1T-TaS_2: $\chi_0=-1.96\times10^{-7}$ emu/g, $\Theta=0.4$ K, and $C=0.806\times10^{-6}$ emu K/g.[18] These values of χ_0, Θ, and C are comparable to those derived in the present work for Ta_2S_2C. The Curie-type behavior in 1T-TaS_2 is not due to magnetic impurities, but due to the localized magnetic moments related to the Anderson localization effect.[18,19] The diamagnetic susceptibility is common to the 1T-polytypes showing CDW's. In 1T-TaS_2, the effect of the ordering of the commensurate CDW below 200 K is clearly observed in a discontinuous jump in the electrical resistivity.[18,19] In Ta_2S_2C the T dependence of the electrical resistivity ρ has been reported by Ziebarath *et al.*[3] using a pressed- and sintered-sample. The resistivity increases with increasing T for $4.2\leqslant T\leqslant300$ K ($\rho\approx0.8$ m Ω cm at 4.2 K and 2.2 m Ω cm at 300 K), showing a metallic behavior. Unlike the resistivity of 1T-TaS_2, no discontinuous change in ρ has been observed below 300 K.

G. M_{ZFC} vs H at low T and high H

Figure 12 shows the H dependence of M_{ZFC} at fixed T below T_{cl}. The magnetization M_{ZFC} is negative at low H because of the Meissner effect. The sign of M_{ZFC} changes to positive at a zero-crossing field $H_0(T)$. The value of H_0 (=5.6 kOe at 1.9 K) coincides with that evaluated from the relation $H_{c2}^{(l)}(T)=H_{c2}^{(l)}(0)[1-(T/T_{cl})^2]$. The magnetization M_{ZFC} increases with further increasing H. It shows a broad peak, which shifts to the high-H side with increasing T: 22.5 kOe at 1.9 K and 29 kOe at 3.5 K. This peak arises from a competition between the Curie-type behavior (ΔM_{ZFC}) and the diamagnetic contribution ($\chi_d H$). In Fig. 13 we show the plot of a magnetization ΔM_{ZFC} as a function of H^*/T, where $\Delta M_{ZFC}=M_{ZFC}-\chi_d H$ with $\chi_d=-1.44\times10^{-7}$ emu/g, and $H=10^4H^*$ (H and H^* are in the units of Oe and Tesla, respectively). The curves of ΔM_{ZFC} vs H^*/T, which are slightly different for different T, increase with increasing H^*/T. The function form of ΔM_{ZFC} vs H^*/T will be discussed in Sec. IV B.

IV. DISCUSSION

A. Origin of successive phase transitions at T_{cl} and T_{cu}

We find that Ta_2S_2C undergoes successive superconducting transitions at T_{cl} and T_{cu}. The diamagnetic volume fraction (21%) indicates that our system is formed of many small grains. The T and H dependence of χ_{ZFC} and χ_{FC} below T_{cl} is very different from that between T_{cl} and T_{cu}: $\delta\chi>0$ for

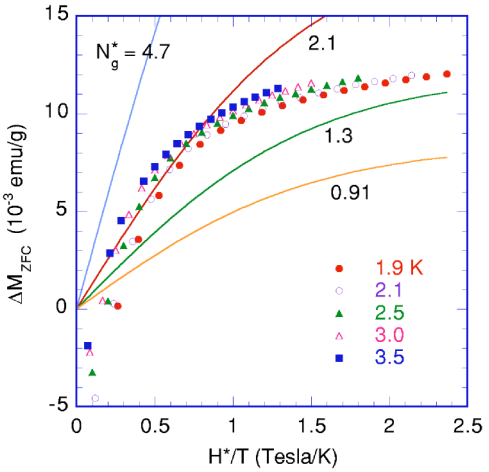

FIG. 13. (Color online) Difference ΔM_{ZFC} ($=M_{ZFC}-\chi_d H$) as a function of H^*/T where $\chi_d=-1.44\times10^{-7}$ emu/g, $H=H^*\times10^4$ (H and H^* are in the units of Oe and Tesla, respectively), and the data of Fig. 12 for M_{ZFC} are used. The solid lines denote Brillouin functions given by $N_g\mu_B\tanh(0.6717H^*/T)$ with $N_g=N_g^*\times10^{18}$/g, where $N_g^*=4.7$, 2.1, 1.3, and 0.91.

$T<T_{cl}$ and $\delta\chi\approx0$ ($\delta\chi>0$) for $T_{cl}<T<T_{cu}$. The difference $\delta\chi$ at a fixed T below T_{cl} decreases with increasing H. In contrast, $\delta\chi$ at a fixed T between T_{cl} and T_{cu} increases with increasing H, showing a maximum around $H=500$ Oe, and decreases with further increasing H. We note that similar successive transitions have been reported in a ceramic superconductor $YBa_2Cu_4O_8$ ($T_{cl}=37$ K and $T_{cu}=80$ K),[26,27] which consists of small grains. Below T_{cu}, χ_{ZFC} ($=\chi_{FC}$) becomes negative. The difference $\delta\chi$ appears below T_{cl}. The difference $\delta\chi$ at a fixed T below T_{cl} decreases with increasing H.

The successive phase transitions at T_{cl} and T_{cu} in $YBa_2Cu_4O_8$ can be qualitatively explained by Kawachi *et al.*[26] by taking into account the role of the superconducting grain below T_{cu} and clusters below T_{cl}. According to their model, our results of Ta_2S_2C can be explained as follows. Below T_{cu} the superconductivity occurs in each grain. In the presence of H well above $H_{c1}^{(u)}$, the fluxoids are pinned by pinning centers such as defects and vacancies within grains. A very weak irreversible effect of magnetization suggests that the density of fluxoids pinned in each grain for the FC state is slightly larger than the ZFC state. The distribution of fluxoids in the FC state is more uniform, while in the ZFC state more fluxoids are concentrated in the grain-boundary, which does not contribute to χ_{ZFC}.[28,29] Below T_{cl}, the superconductivity occurs in clusters formed of grains coupled through weak intergrain Josephson couplings. In the presence of H, the system is divided into relatively free regions (the cluster-boundary region) and strong-pinned regions (within the clusters). In the FC state, the distribution of the fluxoids is more uniform inside the clusters. In the ZFC state, more fluxoids are concentrated in the cluster-boundary regions which may have little contribution to χ_{ZFC}. In the presence of $H(<H_{c1}^{(l)})$ applied to the system in the ZFC state, the fluxoids will enter only the cluster-boundary regions around the clusters. The fluxoids in the intercluster region can have a path through the system without being caught by clusters.

When $H > H_{c1}^{(l)}$, some free fluxoids are caught by the clusters and pinned strongly, which contributes to χ_{ZFC}. Because of such an increase in χ_{ZFC}, $\delta\chi$ decreases with increasing H.

The possible existence of mesoscopic grains in the Ta-C layers of Ta_2S_2C would be essential to the successive transitions having a hierarchical nature. The superconductive ordering proceeds in two steps from the intraplanar Josephson couplings between grains in the same Ta-C layers to the interplanar Josephson interaction between grains in adjacent Ta-C layers separated by TaS_2-type structure. In the intermediate phase between T_{cu} and T_{cl}, each grain in Ta-C layers becomes a superconductor. Through the intraplanar Josephson coupling between grains, the region of the superconducting grains becomes larger as T decreases below T_{cu}, forming a 2D superconducting phase. Thermal fluctuations overcome the interplanar Josephson coupling. Just below T_{cl}, the effective interplanar Josephson coupling becomes strong enough to give rise to a 3D superconducting phase. The 2D superconducting systems are coupled to each other through a weak interplanar Josephson coupling between adjacent Ta-C layers.

We note that the magnetic analogy to the successive phase transitions of such a hierarchical nature is seen in a stage-2 $CoCl_2$ graphite intercalation compound (GIC):[30] T_{cu} (=8.9 K) and T_{cl} (=6.8–7.2 K). The existence of islands is essential to the successive phase transitions. The nearest neighbor spins inside islands are ferromagnetically coupled with intraplanar exchange interactions. On approaching T_{cu} from the high-T side, spins come to order ferromagnetically inside islands. At T_{cu} these ferromagnetic islands continue to order over the same layer through interisland interactions (mainly ferromagnetic), forming a 2D ferromagnetic long-range order. Below T_{cl} a reentrant spin-glasslike phase order is established through effective antiferromagnetic interplanar interactions between spins in adjacent intercalate layers, where the antiferromagnetic phase and the spin glass phase coexist.

B. Anderson localization effect

We have shown that in Ta_2S_2C, the susceptibility χ_{FC} at low T and high H obeys the Curie law, which is a direct evidence of the appearance of local magnetic moments of unpaired electrons due to the Anderson localization effect. A theory for the magnetic susceptibility in systems with both localization and electron-electron interactions is presented by Kobayashi *et al.*,[31] and Kamimura and Aoki.[32] It is assumed that there are localized states with energies very close to the Fermi level ϵ_F. Single occupied states are energetically favorable by virtue of intrastate Coulomb interaction ($U>0$) between spin-up and spin-down electrons in the same localized state. In the presence of H, the magnetization contribution m_i of the ith localized state with energy ϵ_i, relative to ϵ_F, can be written as

$$m_i = \mu_B[e^{-\beta(\epsilon_i-\mu_B H)} - e^{-\beta(\epsilon_i+\mu_B H)}]/Z, \tag{2}$$

where $\beta=1/(k_B T)$, μ_B is the Bohr magneton, and Z is the partition function given by

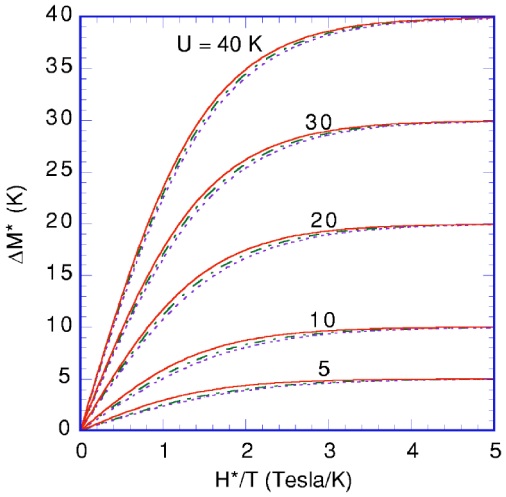

FIG. 14. (Color online) Plot of $\Delta M^*=(M_e-M_P)/(k_B N(0)\mu_B)$ for $T=1.9$ K (dashed-dotted line) and $T=3.5$ K (dotted line), and the Brillouin function given by $M_B^*=U\tanh(\mu_B H/k_B T)$ (solid line) as a function of H^*/T as the intrastate Coulomb interaction U (in the units of K) is changed as a parameter. $U=27$ K for 1T-TaS_2 (Ref. 19). M_e is defined by Eq. (4). M_P is the Pauli paramagnetism given by $M_P=2N(0)\mu_B^2 H$.

$$Z = 1 + e^{-\beta(\epsilon_i-\mu_B H)} + e^{-\beta(\epsilon_i+\mu_B H)} + e^{-\beta(2\epsilon_i+U)}, \tag{3}$$

corresponding to an empty state, a state occupied by a spin-up electron with the energy $\epsilon_i-\mu_B H$, a state occupied by a spin-down electron with the energy $\epsilon_i+\mu_B H$, and a state occupied by spin-up and spin-down electrons with 2 ϵ_i+U. Then the total magnetization M_e is obtained as

$$M_e = \frac{N(0)\mu_B \sinh(\beta\mu_B H)}{\beta[\cosh^2(\beta\mu_B H) - e^{-\beta U}]^{1/2}} \times \ln\frac{\cosh(\beta\mu_B H) + [\cosh^2(\beta\mu_B H) - e^{-\beta U}]^{1/2}}{\cosh(\beta\mu_B H) - [\cosh^2(\beta\mu_B H) - e^{-\beta U}]^{1/2}}, \tag{4}$$

where $N(0)$ is the density of states at ϵ_F. For $U=0$, M is equal to the Pauli paramagnetism $M_P=2N(0)\mu_B^2 H$. Here we define ΔM^* as $\Delta M^*=(M_e-M_P)/(k_B N(0)\mu_B)$, where H is in the unit of Oe and U is in the unit of K: $U=27$ K for the pristine 1T TaS_2. Figure 14 shows the plot of ΔM^* as a function of H^*/T for $0\leqslant H^*\leqslant 10$ T and $T=1.9$ and 3.5 K as U is changed as a parameter, where H^* is in the units of Tesla. For comparison, the Brillouin function given by $M_B^*=U\tanh(\beta\mu_B H)$ is also plotted for each U. Although ΔM^* depends on both H^*/T and U/T for each U, the curve of ΔM^* vs H^*/T for each U fits well with M_B^* with the same U. Note that M_B^* is a little larger than ΔM^* at the same H^*/T for $0\leqslant H^*/T\leqslant 3$. The magnetization ΔM^* at $H^*/T=5$ is equal to the saturation magnetization ($=U$) of M_B^*. This implies that ΔM^* with U coincides with the magnetization of free electron spins whose number is given by $N(0)U$.

Here we discuss our result shown in Fig. 13 based on the above model. As shown Fig. 13, all the data of ΔM_{ZFC} vs H^*/T do not fall on a single-valued function of H^*/T. This is consistent with the expression given by Eq. (4). Negative values of ΔM_{ZFC} for $H^*/T<0.3$ are due to the Meissner

effect. In Fig. 13 a solid line denotes a Brillouin function given by $N_g\mu_B \tanh(0.6717H^*/T)$ with $N_g\mu_B=0.019$ emu/g or $N_g=2.1\times10^{18}$/g, where $N_g=N(0)U$. Our data of ΔM_{ZFC} vs H^*/T greatly deviates downward from this Brillouin function for $H^*/T>1$. In Fig. 13 the magnetization ΔM_{ZFC} reaches 0.012 emu/g at $H^*/T=2.5$. Since the saturation magnetization is $N_g\mu_B$, the value of N_g can be estimated as $N_g=1.3\times10^{18}$/g. We also note $N_g=4.7\times10^{18}$/g ($N_g\mu_B=0.044$ emu/g) in the limit of $H^*/T\rightarrow0$, which is evaluated from the Curie-Weiss constant (see Sec. III F). Alternative method to determine N_g is as follows. We assume that $M_{\mathrm{ZFC}}=\chi_d H+N_g\mu_B \tanh(\beta\mu_B H)$. The magnetization M_{ZFC} at fixed T_1 has a local maximum at $H^*=H_1^*$: $N_g=-1.6053\times10^{24}\ T\chi_d \cosh^2(0.671713H_1^*/T_1)$. Using the values of H_1^* and T_1 determined from the inset of Fig. 12 and $\chi_d=-1.44\times10^{-7}$ emu/g, N_g is calculated as $N_g=(0.91\pm0.05)\times10^{18}$/g. This value of N_g is close to that for 1 T-TaS_2 ($N_g=1.3\times10^{18}$/g) which is calculated from the Curie-Weiss constant ($C_g=0.806\times10^{-6}$ emu/g) obtained by DiSalvo and Waszczak.[18] For comparison, in Fig. 13 we also show the Brillouin function with these values of N_g, as a function of H^*/T. We do not find any reasonable value of N_g, which leads to good agreement between the result and the Brillouin function over the whole range of H^*/T. Similar behavior has also been observed in 1T-TaS_2: the downward deviation of the observed magnetization from the Brillouin function (corresponding to the case of $N_g=2.1\times10^{18}$/g in Fig. 13) occurs for $H^*/T\geqslant0.25$.[19] One of the reason for such a difference between the theory and experiment is that that U is assumed to be constant in the above model. The intrastate Coulomb energy $U_i=U(\epsilon_i)$ is considered to decrease with increasing ϵ_i. The total energy $2\epsilon_i+U_i$ is needed for the state i to be occupied by the spin-up and spin-down electrons. If $2\epsilon_i+U_i>0$, the ith state is occupied by a single electron which behaves as a free spin. If $2\epsilon_i+U_i<0$, the ith state is occupied by paired electrons.[33] The number of free spins is given by $N(0)\Delta U$, where ΔU is the region where free spins can situate on the localized states. The replacement of U by ΔU ($<U$) leads to a decrease in the saturation magnetization. Thus the downward deviation of the magnetization from the Brillouin function with U in Ta_2S_2C and 1T-TaS_2 can be qualitatively explained in terms of this replacement.

V. CONCLUSION

Two phenomena (the superconductivity and the Anderson localization effect) are observed in Ta_2S_2C. The structure of Ta_2S_2C can be viewed as a sum of Ta-C layers and TaS_2-type structure. The superconductivity is mainly due to the Ta-C layers, while the Anderson localization effect is due to TaS_2-type structure. Ta_2S_2C undergoes successive superconducting transitions of a hierachical nature at $T_{cl}=3.61\pm0.01$ K and $T_{cu}=8.9\pm0.1$ K. The intermediate phase between T_{cu} and T_{cl} is an intragrain superconductive state occurring in the Ta-C layers in Ta_2S_2C, while the low temperature phase below T_{cl} is an intergrain superconductive state. The T dependence of magnetic susceptibility at H well above 10 kOe and the H dependence of M_{ZFC} at low T and high H are described by a sum of a diamagnetic susceptibility and a Curie-type behavior. The latter shows that the Anderson localization effect occurs in the 1T-TaS_2-type structure in Ta_2S_2C, leading to the localized magnetic moments due to unpaired electrons just below ϵ_F.

ACKNOWLEDGMENTS

The authors are grateful to Pablo Wally, Technical University of Vienna, Austria (now Littlefuse, Yokohama, Japan) for providing them with the samples. One of the authors (J.W.) acknowledges financial support from the Ministry of Cultural Affairs, Education and Sport, Japan, under the grant for young scientists No. 70314375 and from Kansai Invention Center, Kyoto, Japan.

*Electronic address: juergen.walter@chemiemetall.de; CM Chemiemetall GmbH, Niels-Bohr-Str. 5, Bitterfeld, Germany.
†Electronic address: itsuko@binghamton.edu
‡Electronic address: suzuki@binghamton.edu

[1] R. Brec, J. Ritsma, G. Ouvrard, and J. Rouxel, Inorg. Chem. **16**, 660 (1977).
[2] H. Boller and H. Blaha, J. Solid State Chem. **45**, 119 (1982).
[3] R. P. Ziebarath, J. K. Vassiliou, and F. J. DiSalvo, J. Less-Common Met. **156**, 207 (1989).
[4] H. Boller and K. Hiebl, J. Alloys Compd. **183**, 438 (1992).
[5] H. Boller, Int. J. Refract. Met. Hard Mater. **12**, 195 (1993–1994).
[6] P. Wally and M. Ueki, J. Solid State Chem. **138**, 250 (1998).
[7] P. Wally and M. Ueki, J. Alloys Compd. **268**, 83 (1998).
[8] P. Wally and M. Ueki, Wear **215**, 98 (1998).
[9] J. Walter, H. Shioyama, and S. Hara, J. Vac. Sci. Technol. B **18**, 1203 (2000).
[10] J. Walter, W. Boonchuduang, and S. Hara, J. Alloys Compd. **305**, 259 (2000).
[11] K. Sakamaki, H. Wada, H. Y. Ōnuki, and M. Kawai, Solid State Commun. **118**, 113 (2001).
[12] A. L. Giorgi, E. G. Szklarz, E. K. Storms, A. L. Bowman, and B. T. Matthias, Phys. Rev. **125**, 837 (1962).
[13] H. J. Fink, A. C. Thorsen, E. Parker, V. F. Zackay, and L. Toth, Phys. Rev. **138**, A1170 (1965).
[14] C. Oshima, R. Souda, M. Aono, S. Otani, and Y. Ishizawa, Phys. Rev. Lett. **56**, 240 (1986), and references therein.
[15] I. S. Suzuki, M. Suzuki, and J. Walter, Solid State Commun. **118**, 523 (2001).
[16] A. Wilson, F. J. DiSalvo, and S. Mahajan, Adv. Phys. **24**, 117 (1975).
[17] F. J. DiSalvo and J. E. Graebner, Solid State Commun. **23**, 825 (1977).
[18] F. J. DiSalvo and J. V. Waszczak, Phys. Rev. B **22**, 4241 (1980).
[19] R. Inada, Y. Ōnuki, and S. Tanuma, J. Phys. Soc. Jpn. **50**, 1217 (1981).
[20] See for example, J. B. Ketterson and S. N. Song, *Superconduc-*

tivity (Cambridge University Press, Cambridge, 1999).
[21] P. Kostić, B. Veal, A. P. Paulikas, U. Welp, V. R. Todt, C. Gu, U. Geiser, J. M. Williams, K. D. Carlson, and R. A. Klemm, Phys. Rev. B **53**, 791 (1996).
[22] L. Pust, L. E. Wenger, and M. R. Koblischka, Phys. Rev. B **58**, 14 191 (1998).
[23] A. E. Koshelev and A. I. Larkin, Phys. Rev. B **52**, 13 559 (1995).
[24] N. R. Werthamer, E. Helfand, and P. C. Hohenberg, Phys. Rev. **147**, 295 (1966).
[25] R. C. Morris and R. V. Coleman, Phys. Rev. B **7**, 991 (1973).
[26] M. Kawachi, M. Hagiwara, K. Koyama, and M. Matsuura, J. Phys. Soc. Jpn. **63**, 3405 (1994).
[27] M. Matsuura, M. Kawachi, K. Miyoshi, M. Hagiwara, and K. Koyama, J. Phys. Soc. Jpn. **64**, 4540 (1995).
[28] L. Ji, M. S. Rzchowski, and M. Tinkham, Phys. Rev. B **42**, 4838 (1990).
[29] L. Ji, M. S. Rzchowski, N. Anand, and M. Tinkham, Phys. Rev. B **47**, 470 (1993).
[30] M. Suzuki and I. S. Suzuki, Phys. Rev. B **58**, 840 (1998).
[31] S. Kobayashi, Y. Fukagawa, S. Ikehata, and W. Sasaki, J. Phys. Soc. Jpn. **45**, 1276 (1978).
[32] H. Kamimura and H. Aoki, *The Physics of Interacting Electrons in Disordered Systems* (Clarendon, Oxford 1989), and references therein for the Anderson localization effect.
[33] S. Ikehata, T. Ema, S. Kobayashi, and W. Sasaki, J. Phys. Soc. Jpn. **50**, 3655 (1981).